NANO LETTERS

Letter

pubs.acs.org/NanoLett

Multicolor Silicon Light-Emitting Diodes (SiLEDs)

Florian Maier-Flaig,*[,†] Julia Rinck,[‡] Moritz Stephan,[†] Tobias Bocksrocker,[†] Michael Bruns,[§,∥] Christian Kübel,[∥,⊥] Annie K. Powell,[‡,⊥,#] Geoffrey A. Ozin,*[,‡,▽] and Uli Lemmer*[,†]

[†]Light Technology Institute (LTI) and DFG Center for Functional Nanostructures, Karlsruhe Institute of Technology (KIT), Kaiserstraße 12, 76131 Karlsruhe, Germany

[‡]DFG Center for Functional Nanostructures (CFN), Karlsruhe Institute of Technology (KIT), Wolfgang-Gaede Straße 1a, 76131 Karlsruhe, Germany

[§]Institute for Applied Materials (IAM-ESS), [∥]Karlsruhe Nano Micro Facility (KNMF), and [⊥]Institute of Nanotechnology (INT), Karlsruhe Institute of Technology (KIT), Hermann-von-Helmholtz-Platz 1, 76344 Eggenstein-Leopoldshafen, Germany

[#]Institute of Inorganic Chemistry, Karlsruhe Institute of Technology (KIT), Engesserstraße 15, 76131 Karlsruhe, Germany

[▽]Department of Chemistry, University of Toronto, 80 St. George Street, Toronto, ON, Canada M5S 3H6

S *Supporting Information*

ABSTRACT: We present highly efficient electroluminescent devices using size-separated silicon nanocrystals (ncSi) as light emitting material. The emission color can be tuned from the deep red down to the yellow-orange spectral region by using very monodisperse size-separated nanoparticles. High external quantum efficiencies up to 1.1% as well as low turn-on voltages are obtained for red emitters. In addition, we demonstrate that size-separation of ncSi leads to drastically improved lifetimes of the devices and much less sensitivity of the emission wavelength to the applied drive voltage.

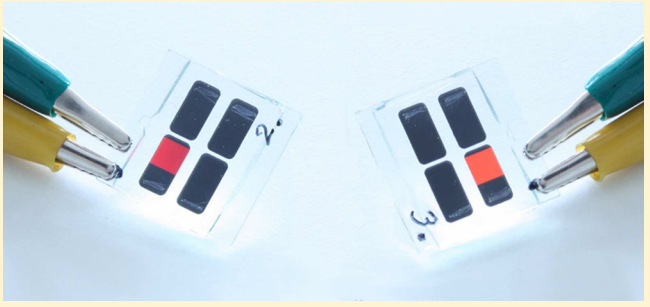

KEYWORDS: *Silicon nanocrystals, quantum dot light-emitting diodes (QD-LEDs), quantum dot, electroluminescence, tunable color, hybrid organic quantum dot light-emitting diode (hybrid QD-OLED)*

Semiconductor quantum dots (QDs) are a new emerging class of materials combining tailored electronic properties and the advantageous ability to be processed out of solution with common printing and coating techniques. Colloidally stable QDs are therefore expected to find widespread application in electronics and optoelectronics such as light-emitting diodes (LEDs)[1−12] and solar cells.[13] Even though QD-LEDs have been intensively investigated,[3,10−12] the toxicity of the elements used for efficient II−VI QD-LEDs, such as CdS, CdSe, and their Pb containing counterparts, is a severe drawback for many applications. In contrast, silicon nanocrystals (ncSi) seem to be ideally suited due to the nontoxicity and abundance of this element which is dominating the whole microelectronics and photovoltaics industry. As bulk silicon is an indirect semiconductor significant light emission is only achieved under strong confinement conditions occurring for ncSi with a size of about 5 nm or less.[14] The recent reports on very high photoluminescence quantum yields,[15,16] novel synthesis routes, colloidal stability of ncSi, and indications of no cytotoxicity of ncSi[17,18] has drawn much attention to the exploration of LEDs based on silicon nanocrystals.[6−8] Although red and NIR light-emitting diodes were recently realized[6−9] and have shown the large potential of Si based QD-LEDs, the major challenge is still to explore pathways for efficient devices covering the whole visible range.

In this study, we introduce bright, long-term stable and color-tunable silicon light-emitting diodes (SiLEDs) featuring intense electroluminescence (EL) from the NIR down to the yellow spectral region by using size-separated ncSi. The nanocrystals are capped with allylbenzene and produced by solid-state synthesis.[19] Details of our synthetic approach are reported in the Supporting Information. The resulting particles are colloidally stable in toluene, feature sizes in the range of 1−3 nm, and exhibit photoluminescence quantum yields of up to 43%.[15] Directly after synthesis, the as-prepared ncSi solutions were size-separated by size-selective precipitation using the method reported in ref 15.

Under UV-illumination the size-separated ncSi-solutions emit over a broad spectral range from the NIR down to the yellow/green spectral region (see Figure 1a). Out of these solutions, three representative samples were chosen for the experiments described in the following. The particles show bright and intense photoluminescence (PL) with peaks at 680, 650, and 625 nm, corresponding to approximately 1.8, 1.6, and 1.3 nm sized ncSi.[15] The corresponding PL spectra are shown

Received: October 19, 2012
Revised: January 11, 2013
Published: January 15, 2013

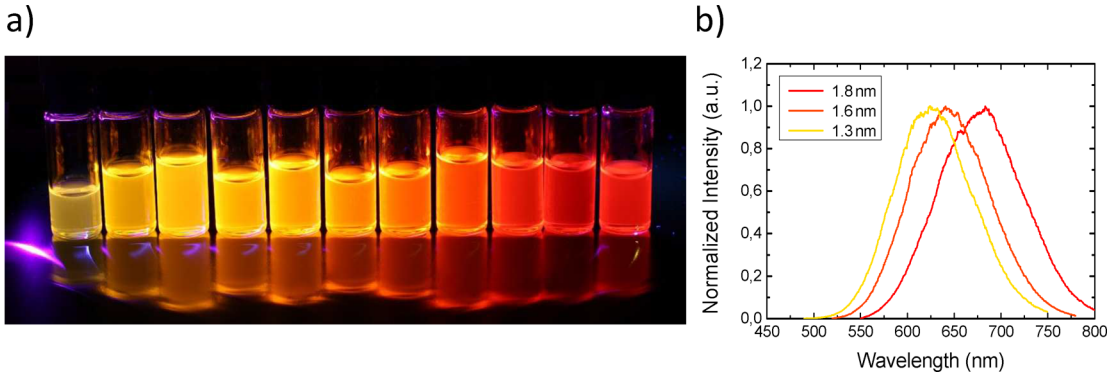

Figure 1. Size-separated silicon nanocrystals (ncSi) and their corresponding PL spectra. (a) Nanoparticles dispersed in toluene showing intense luminescence from the deep red to the yellow spectral region. (b) PL spectra of the three samples used for SiLED fabrication. Excitation: (a) 365 nm LED and (b) 355 nm Nd:YAG laser.

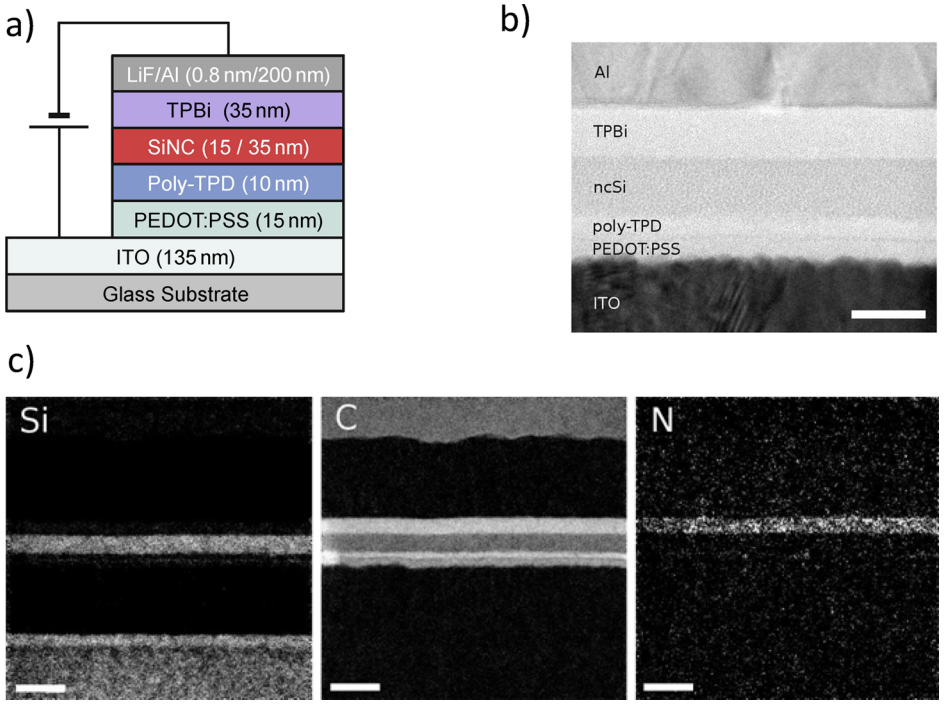

Figure 2. Device architecture and morphology of SiLED structure. (a) Schematic view of SiLED stack. (b) BF-TEM image showing the layer structure of a real device (scale bar: 50 nm). (c) EFTEM images of a SiLED cross-section. The silicon, carbon, and nitrogen elemental maps are obtained using the three-window technique (scale bar: 100 nm).

in Figure 1b and clearly show the shift of the emission wavelength for particles of different sizes.

Figure 2a depicts the LED stack of the devices used in this study. All SiLEDs were built by spin-coating of the different functional layers on lithographically structured ITO-covered glass substrates followed by a thermal evaporation step of the cathode. Before liquid processing of the different layers, the substrates are cleaned with acetone and isopropanol in an ultrasonic bath followed by a 2 min oxygen plasma treatment. A 15 nm thick layer of poly(3,4-ethylenedioxythiophene):poly-(styrenesulfonate) (PEDOT:PSS, Baytron P VPAI 4083) is then spin-coated (500 rpm (3 s), 4000 rpm (55 s)) on top of the as-prepared substrate followed by a thin hole-transport layer (HTL) of poly(*N*,*N*′-bis(4-butylphenyl)-*N*,*N*′-bis(phenyl)-benzidine (poly-TPD, ADS254BE, 8.5 mg/mL, 1500 rpm (55 s), 4000 rpm (2 s)) which was dissolved in toluene. Subsequently, pure toluene is spin-coated (1500 rpm (40 s)) on the samples to reduce the poly-TPD layer thickness. The remaining thickness is around 10 nm and is not directly measurable using a Dektak profilometer. However, the layer still shows strong PL related to the polymer. On the emissive layer (1000 rpm (50 s), 4000 rpm (2 s)), a 35 nm thick hole-blocking layer (HBL) of 1,3,5-tris(*N*-phenylbenzimidazol-2,yl)benzene (TPBI) followed by a 0.8 nm/200 nm thick layer of LiF/Al is thermally evaporated.

For characterization the devices are encapsulated using a thin glass slide and epoxy adhesive. Characterization was done using an integrating sphere coupled to a spectrometer with an attached ICCD camera. For further details see Supporting Information.

Figure 2a depicts the LED stack of the devices used in this study. The bright-field TEM (BF-TEM) image of a cross section of a real device is shown in Figure 2b. The different organic layers as well as the ncSi layer can be clearly

dx.doi.org/10.1021/nl3038689 | *Nano Lett.* 2013, 13, 475−480

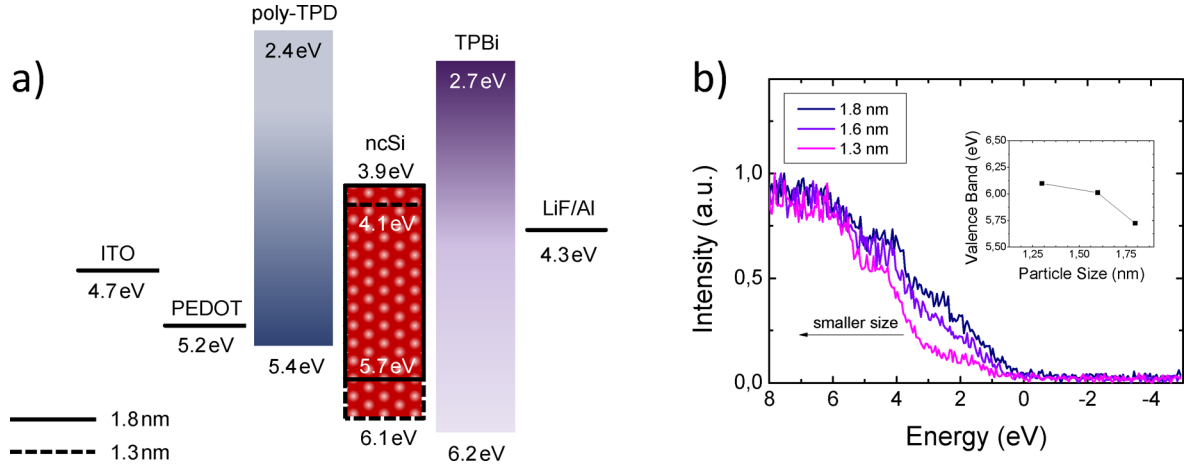

Figure 3. Band diagram of the materials used in devices as well as valence band as a function of the nanoparticle size determined by XPS. (a) Band diagram of the SiLED stack, energy values of ncSi are determined by XPS others are taken from literature. (b) Normalized XPS spectra of the nanoparticles used in this study. As shown in the inset, a strong increase of valence band E_{VB} for decreasing particle size and emission wavelength is observed.

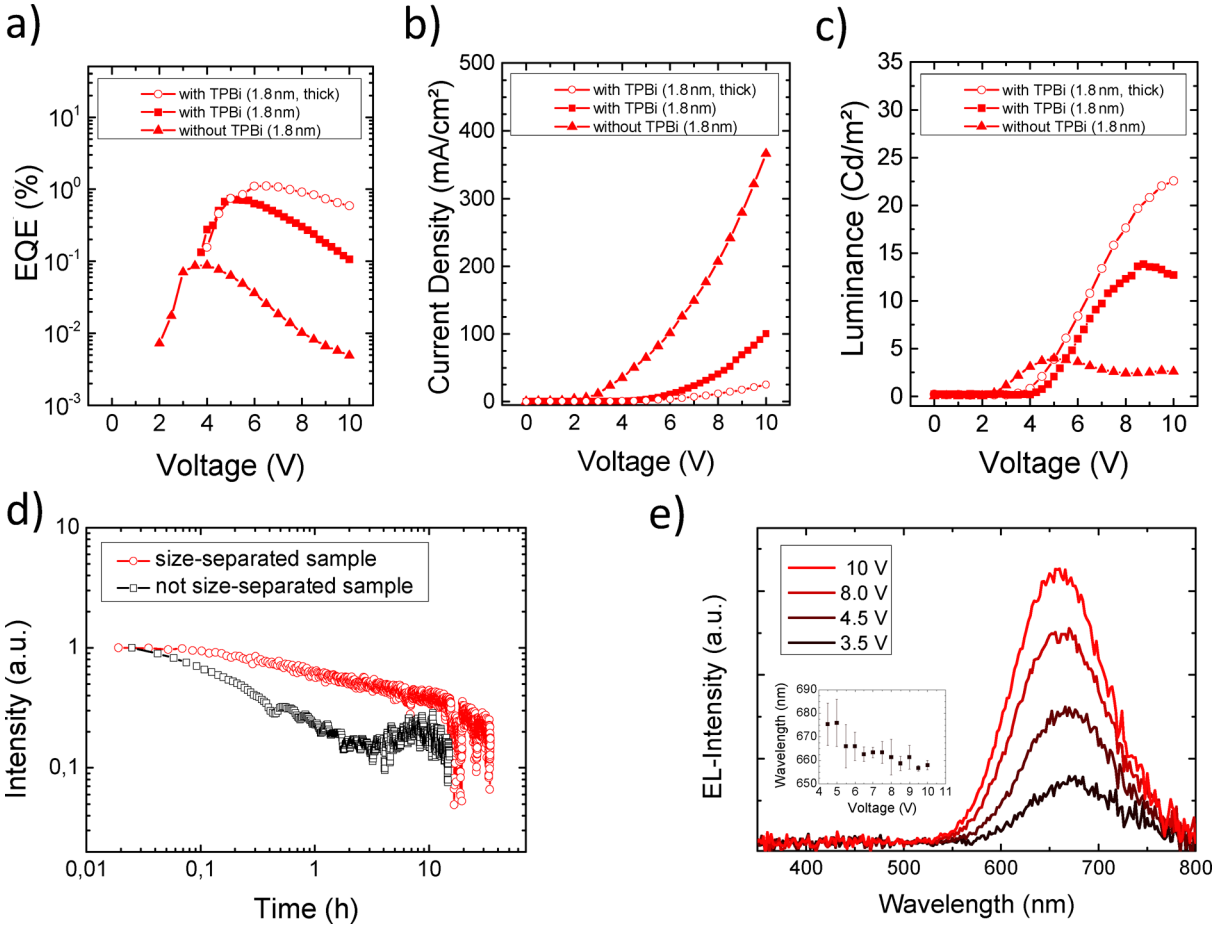

Figure 4. Device performance of SiLEDs. (a) External quantum efficiency (EQE), (b) JV characteristics, and (c) luminance–voltage characteristics of devices built with/without TPBI (ncSi emissive layer: ~30 nm) compared to SiLEDs using TPBI and a thick emissive layer of about 35 nm. (d) EL intensity over time at constant current of 1.6 mA/cm^2. (e) EL spectra as a function of applied voltage (3.5, 4.5, 8, and 10 V). Only a minor shift of about 15 nm is observed for devices using size-separated samples. The inset shows a shift of the EL maximum averaged over three different SiLEDs.

distinguished and are in good agreement with the nominal layer structure. The results of BF-TEM imaging are further confirmed by energy filtered TEM (EFTEM) imaging, as depicted in Figure 2c. All layers are spatially well-defined, exhibit smooth interfaces, and can be clearly attributed to the different materials used. The ncSi layer features a strong Si-related contrast as well as the carbon signature of the organic ligands. The carbon fingerprint is significantly more pro-

dx.doi.org/10.1021/nl3038689 | Nano Lett. 2013, 13, 475–480

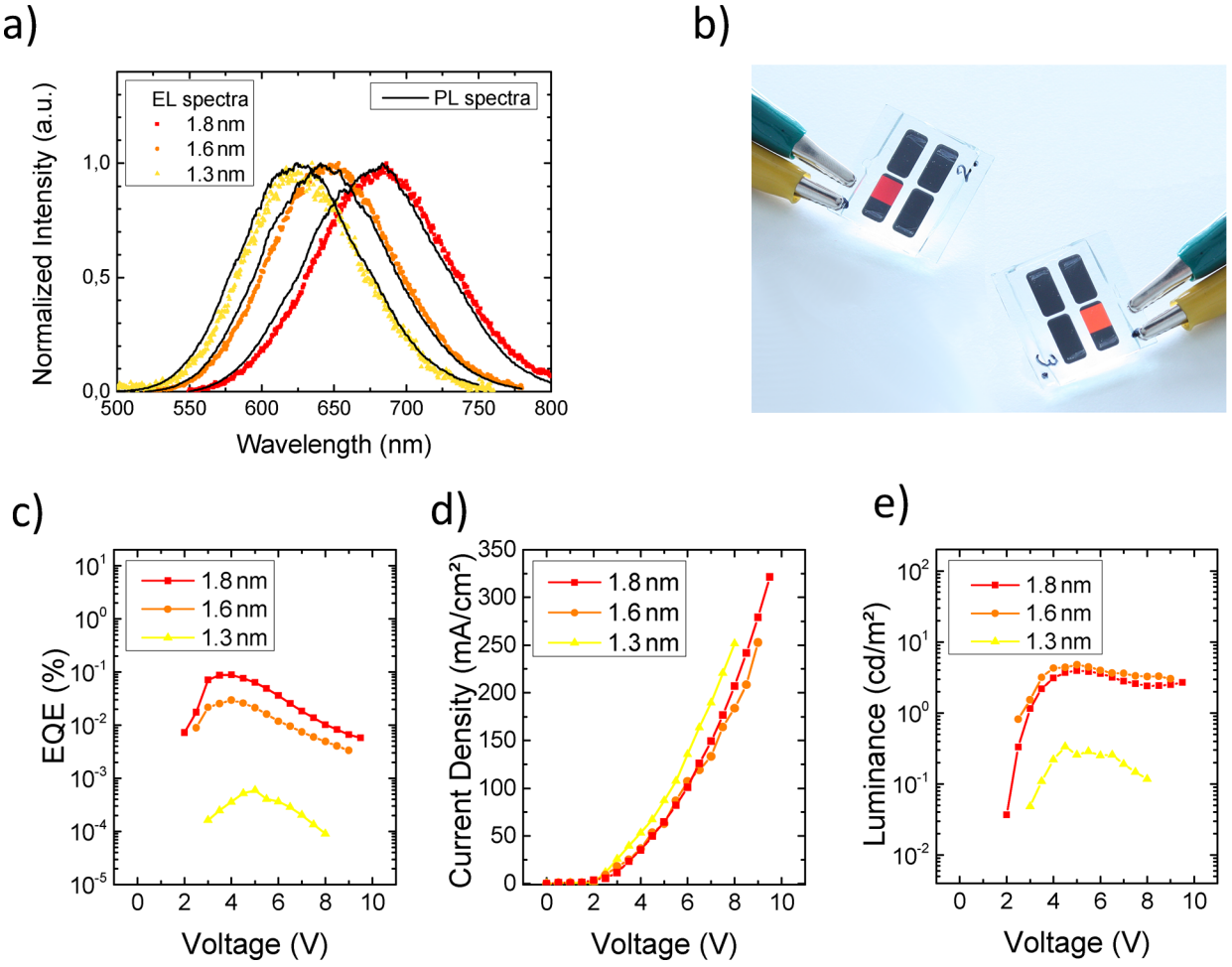

Figure 5. Optoelectronic parameters of SiLEDs featuring different emission wavelengths. (a) Comparison of EL and PL of different-sized emitters. (b) SiLEDs connected to a 9 V battery in series to an ohmic resistor limiting the voltage to 6 V. The individual photographs are taken at ambient lighting conditions and are not modified with any image processing software. (c) External quantum efficiency (EQE), (d) JV characteristics, and (e) luminance–voltage characteristics of devices containing different-sized ncSi as emitters.

nounced in the purely organic layers. N clearly maps the TPBi layer.

In Figure 3a we show the respective band diagram of the SiLEDs. The hole-transport/electron-blocking (HTL/EBL, poly-TPD) and hole-blocking layers (HBL, TPBI) are used to effectively confine injected carriers in the emitting layer leading to an efficient radiative recombination of electrons and holes.[8,20] To achieve the necessary confinement of carriers in the emitting layer it is crucial to determine valence (VB) and conduction band (CB) of the different sized ncSi emitters. In Figure 3b, we therefore show the X-ray photoelectron spectroscopy (XPS) spectra of the three samples used in this work as well as valence band energy (E_{VB}) as a function of the ncSi size (inset Figure 3b). In agreement with theoretical findings,[21−23] the E_{VB} shifts toward higher energies as the nanocrystal size decreases. Large particles (emission wavelength around 680 nm) feature E_{VB} = 5.7 eV, whereas small ncSi show values up to E_{VB} = 6.1 eV. Similar to the case of chalcogenide QDs, we attribute the observed shift of E_{VB} to a change in the electronic *and* morphological structure of ncSi.[24,25] All details on the experimental aspects of XPS and TEM characterization are given in the Supporting Information.

Using now the above shown 1.8-nm-sized ncSi we present the performance of red-emitting SiLEDs featuring high external quantum efficiency (EQE) values. We compare devices built with and without TPBI as HBL keeping the ncSi-layer thickness fixed at 30 nm. In addition we show that increasing the thickness of the emitting ncSi layer leads to even higher EQE values.

As mentioned before and also detailed in ref 8 and 20, EBL and HBL play an important role in terms of device performance. In Figure 4a we show that an increase of EQE about 1 order of magnitude (0.74% vs 0.09%) can be achieved when TPBI is used as HBL. However, this increase comes along with an increased turn-on voltage (see Figure 4b, Figure S1). For a fixed thickness of the ncSi-layer of 30 nm, the device built without HBL already turns on at around 2.0 V, whereas for TPBI devices the turn-on voltage is about 4 V. A further increase of the EQE performance can be achieved when thicker ncSi layers are used. In this case, electron and hole transport is more balanced, leading to an even more efficient radiative recombination. As shown in Figure 4a (empty circles), an approximately 35 nm thick ncSi layer yields 1.1% EQE, representing a world record value for red-emitting SiLEDs. The corresponding luminance values are shown in Figure 4c. The maximum brightness values of the different investigated SiLEDs are 22.6 Cd/m^2 at 10 V (with TPBI, thick layer), 13.8 Cd/m^2 at 8.75 V (with TPBI), and 4.0 Cd/m^2 at 5 V (without TPBI).

dx.doi.org/10.1021/nl3038689 | *Nano Lett.* 2013, 13, 475−480

Despite significant progress in silicon-based LEDs, the long-term stability of these devices under operating conditions is still a challenge and one of the most important fields for further improvement of these devices. While previous work on SiLEDs focused on ncSi samples which have not been size-selected, our devices benefit from quasi monodisperse samples.[15] To compare the performance of SiLEDs built with and without size-separated samples, we plot the lifetime characteristics of these devices in Figure 4d. Size-separation significantly improves the long-term stability of the devices. For size-separated devices operation times of over 40 h are achieved, whereas for not size-separated samples only 15 h of operation are measured. The corresponding (1/e)-lifetime is significantly increased by a factor of 30.

In the case of the nonsize-separated ncSi ensemble, we attribute the significantly shorter lifetimes to large particles which cause short circuits inside the devices and lead to a rapid degradation of the SiLEDs. Furthermore, devices based on nonsize-separated samples show strongly inhomogeneous luminous areas due to impurities and defects.

Figure 4e shows the EL of a device as a function of the applied voltage. In contrast to large shifts of the EL maximum when nonsize-separated ncSi is used,[8] we observe only a small shift of about 15 nm when the applied voltage is increased from 3.5 to 10 V. We assign this small remaining shift to a residual size distribution even after size separation. This shift however can be avoided by either finer separation steps or other more elaborated size-separation methods as shown in ref 26. For comparison, SiLEDs based on nonsize-separated samples show a shift as large as 30 nm (Figure S2, Supporting Information). In summary, Figure 4d–e suggests that lifetimes *and* color-stability of the SiLEDs can be significantly improved using size-separated samples.

In addition to the increased device lifetimes and the small voltage-dependent wavelength shift, size separation enables facile tuning of the emission wavelength. Figure 5a shows the EL of devices built with ncSi of three different sizes (overlaid with the PL already shown in Figure 1b). An excellent agreement between EL and PL of the different emitters is obvious, confirming that emission originates indeed from ncSi. The performance of the devices using the three different ncSi-emitters (layer thickness ~15 nm (yellow/orange), 30 nm (red)) is shown in Figure 5c–e. External quantum efficiency (EQE) values of about 0.1% (at 4 V) are realized for devices containing 680 nm emitting ncSi. The SiLEDs built of ncSi featuring emission wavelengths of 650 and 625 nm show lower EQE which we primarily attribute to the reduced absolute quantum yield (AQY) of the particles.[15] Furthermore, the charge injection as well as carrier confinement in the active layer might be less effective since HOMO and LUMO-levels do not match the ideal configuration anymore (refer to Figure 3 and corresponding paragraph). For comparison reasons these devices were built without TPBI as HBL. TPBI can only be used for devices with ncSi-layers exceeding a critical thickness of more than 20 nm. Otherwise, blue poly-TPD related emission dominates the spectra (Figure S3, Supporting Information). Maximum brightnesses of 3.97 Cd/m^2 (red), 4.77 Cd/m^2 (orange), and 0.34 Cd/m^2 (yellow) were found for the respective devices. Figure 5e depicts the voltage-dependent luminances.

The devices that are shown in Figure 5 feature very low turn-on voltages as low as 1.8 V for red-emitting SiLEDs. This energy, in turn, corresponds practically to the bandgap of the nanoparticles and confirms that almost no energy is lost during the carrier injection process. As shown in Figure 5d the turn-on voltages do not significantly depend on the particles used.

To illustrate the bright, stable, and homogeneous emission of the SiLEDs we show the photographs of two encapsulated devices in Figure 5b. The SiLEDs feature strong red and orange luminescence and can easily be operated under ambient conditions for several hours. To the best of our knowledge, this is the first observation of long-term stable EL of ncSi down to the orange/yellow spectral range.

In conclusion, we demonstrated highly efficient and widely color-tunable SiLEDs. The emission wavelength of the devices can easily be tuned from the deep red (680 nm) down to the orange/yellow (625 nm) spectral region by simply changing the size of the used size-separated ncSi. EQE values as high as 1.1% as well as low turn-on voltages of around 2 V are obtained for red emitters. In addition, we showed that the size of the ncSi has a significant impact on the valence band position of the material. Due to size separation, an increase device lifetime up to at least 40 h of operation as well as a smaller voltage-induced shift of the EL-emission of only 15 nm can be achieved. Using ncSi of well-defined sizes, precisely tunable *and* long-term stable devices can be built which may lead to new silicon-based optoelectronic devices and new applications.

■ ASSOCIATED CONTENT

Ⓢ Supporting Information

A detailed experimental section on the nanoparticle synthesis and devices characterization as well as all details on the experimental aspects of XPS and TEM characterization. Furthermore, two additional figures are provided. This material is available free of charge via the Internet at http://pubs.acs.org.

■ AUTHOR INFORMATION

Corresponding Author

*E-mail: Florian.Maier-Flaig@kit.edu, gozin@chem.utoronto.ca, Uli.Lemmer@kit.edu.

Notes

The authors declare no competing financial interest.

■ ACKNOWLEDGMENTS

G.A.O. is Government of Canada Research Chair in materials chemistry and nanochemistry. He thanks the Natural sciences and Engineering Council of Canada and the Ministry of Science, Research and the Arts of Baden-Württemberg for support of this work at UoT and KIT. F.M.-F. and T.B. acknowledge generous support by the Karlsruhe School of Optics & Photonics (KSOP). We thank Torsten Scherer and Robby Prang at KIT for the FIB sample preparation.

■ REFERENCES

(1) Colvin, V. L.; Schlamp, M. C.; Alivisatos, A. P. *Nature* **1994**, *370*, 354–357.

(2) Tessler, N.; Medvedev, V.; Kazes, M.; Kan, S.; Banin, U. *Science* **2002**, *295*, 1506–1508.

(3) Sun, Q.; Wang, Y. A.; Li, L. S.; Wang, D.; Zhu, T.; Xu, J.; Yang, C.; Li, Y. *Nat. Photonics* **2007**, *1*, 717–722.

(4) Caruge, J. M.; Halpert, J. E.; Wood, V.; Bulovic, V.; Bawendi, M. G. *Nat. Photonics* **2008**, *2*, 247–250.

(5) Cho, K.-S.; Lee, E. K.; Joo, W.-J.; Jang, E.; Kim, T.-H.; Lee, S. J.; Kwon, S.-J.; Han, J. Y.; Kim, B.-K.; Choi, B. L.; Kim, J. M. *Nat. Photonics* **2009**, *3*, 341–345.

(6) Cheng, K.-Y.; Anthony, R.; Kortshagen, U. R.; Holmes, R. J. *Nano Lett.* **2010**, *10*, 1154−1157.
(7) Puzzo, D. P.; Henderson, E. J.; Helander, M. G.; Wang, Z.; Ozin, G. A.; Lu, Z. *Nano Lett.* **2011**, *11*, 1585−1590.
(8) Cheng, K.-Y.; Anthony, R.; Kortshagen, U. R.; Holmes, R. J. *Nano Lett.* **2011**, *11*, 1952−1956.
(9) Anthony, R.; Cheng, K.-Y.; Holman, Z. C.; Holmes, R. J.; Kortshagen, U. R. *Nano Lett.* **2012**, *12*, 2822−2825.
(10) Kwak, J.; Bae, W. K.; Lee, D.; Park, I.; Lim, J.; Park, M.; Cho, H.; Woo, H.; Yoon, D. Y.; Char, K.; Lee, S.; Lee, C. *Nano Lett.* **2012**, *12*, 2362−2366.
(11) Bourvon, H.; Le Calvez, S.; Kanaan, H.; Meunier-Della-Gatta, S.; Philippot, C.; Reiss, P. *Adv. Mater.* **2012**, *24*, 4414−4418.
(12) Sun, L.; Choi, J. J.; Stachnik, D.; Bartnik, A. C.; Hyun, B.-R.; Malliaras, G. G.; Hanrath, T.; Wise, F. W. *Nat. Nanotechnol.* **2012**, *7*, 369−373.
(13) Sargent, E. H. *Nat. Photonics* **2012**, *6*, 133−135.
(14) Canham, L. T. *Appl. Phys. Lett.* **1990**, *57*, 1046−1048.
(15) Mastronardi, M. L.; Maier-Flaig, F.; Faulkner, D.; Henderson, E. J.; Kübel, C.; Lemmer, U.; Ozin, G. A. *Nano Lett.* **2011**, *12*, 337−342.
(16) Jurbergs, D.; Rogojina, E.; Mangolini, L.; Kortshagen, U. *Appl. Phys. Lett.* **2006**, *88*, 233116.
(17) Alsharif, N. H.; Berger, C. E. M.; Varanasi, S. S.; Chao, Y.; Horrocks, B. R.; Datta, H. K. *Small* **2009**, *5*, 221−228.
(18) Wang, Q.; Bao, Y.; Zhang, X.; Coxon, P. R.; Jayasooriya, U. A.; Chao, Y. *Adv. Healthcare Mater.* **2012**, *1*, 189−198.
(19) Henderson, E. J.; Kelly, J. A.; Veinot, J. G. C. *Chem. Mater.* **2009**, *21*, 5426−5434.
(20) Patel, N. K.; Cina, S.; Burroughes, J. H. *IEEE J. Select. Top. Quantum Electron.* **2002**, *8*, 346−361.
(21) Brus, L. J. *J. Chem. Phys.* **1983**, *79*, 5566−5571.
(22) Brus, L. J. *Phys. Chem.* **1986**, *90*, 2555−2560.
(23) Brus, L. J. *Chem. Phys.* **1984**, *80*, 4403−4409.
(24) Colvin, V. L.; Alivisatos, A. P.; Tobin, J. G. *Phys. Rev. Lett.* **1991**, *66*, 2786−2789.
(25) Jasieniak, J.; Califano, M.; Watkins, S. E. *ACS Nano* **2011**, *5*, 5888−5902.
(26) Mastronardi, M. L.; Hennrich, F.; Henderson, E. J.; Maier-Flaig, F.; Blum, C.; Reichenbach, J.; Lemmer, U.; Kübel, C.; Wang, D.; Kappes, M. M.; Ozin, G. A. *J. Am. Chem. Soc.* **2011**, *133*, 11928−11931.
(27) Parry, K. L.; Shard, A. G.; Short, R. D.; White, R. G.; Whittle, J. D.; Wright, A. *Surf. Interface Anal.* **2006**, *38*, 1497−1504.
(28) Hesse, R.; Denecke, R. *Surf. Interface Anal.* **2011**, *43*, 1514−1526.